iScience

CellPress
OPEN ACCESS

Article

NMDAR-mediated activation of pannexin1 channels contributes to the detonator properties of hippocampal mossy fiber synapses

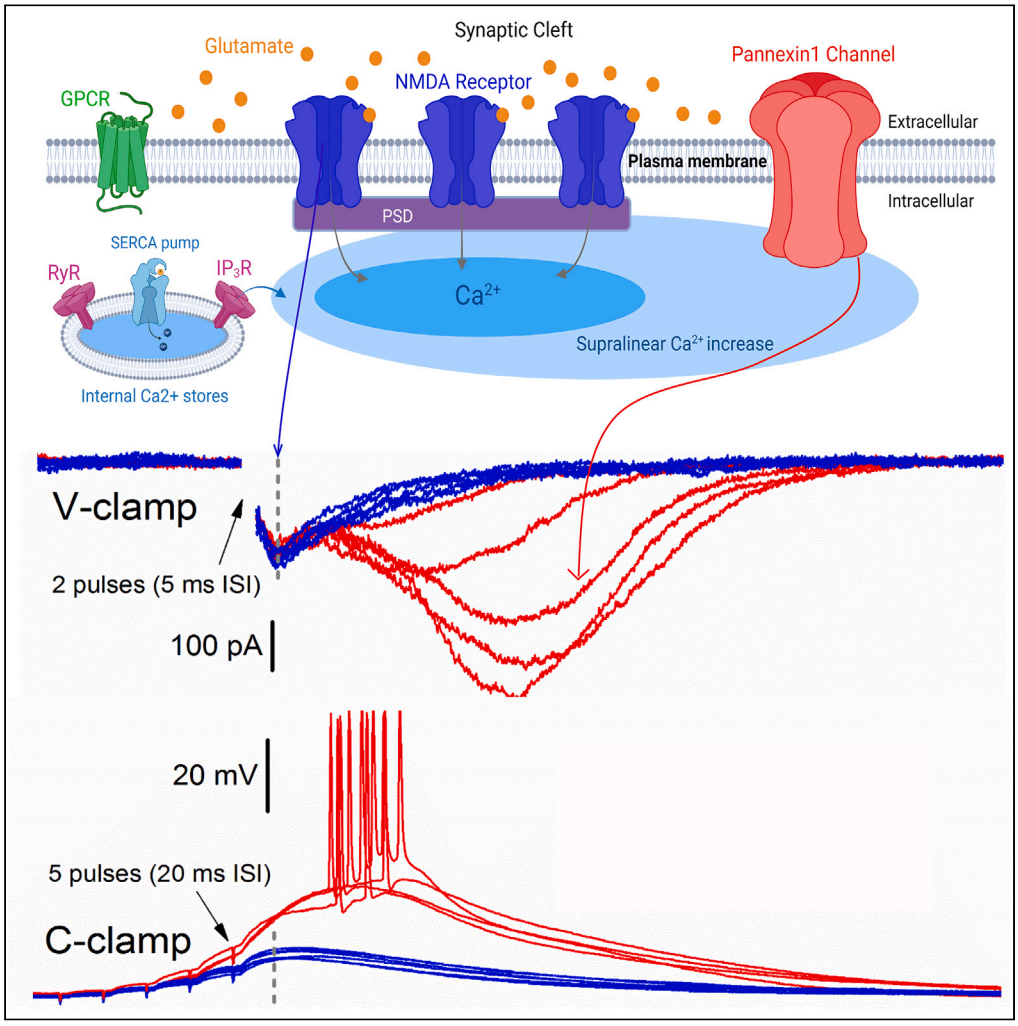

Cinthia Rangel-Sandoval, Marisol Soula, Wei-Ping Li, Pablo E. Castillo, David L. Hunt

pablo.castillo@einsteinmed.edu (P.E.C.)
david.hunt@cshs.org (D.L.H.)

Highlights

NMDA receptor-mediated calcium influx promotes Panx1 channel activation

Panx1 channel activity can be potentiated by metabotropic receptors

Panx1 channel activity can be bidirectionally regulated by NMDAR plasticity

Panx1 activation may contribute to the detonation of CA3 pyramidal neurons

Rangel-Sandoval et al., iScience 27, 109681
May 17, 2024
https://doi.org/10.1016/j.isci.2024.109681

iScience

CellPress
OPEN ACCESS

Article

NMDAR-mediated activation of pannexin1 channels contributes to the detonator properties of hippocampal mossy fiber synapses

Cinthia Rangel-Sandoval,[1,4] Marisol Soula,[2,4] Wei-Ping Li,[3] Pablo E. Castillo,[2,*] and David L. Hunt[1,5,*]

SUMMARY

Pannexins are large-pore ion channels expressed throughout the mammalian brain that participate in various neuropathologies; however, their physiological roles remain obscure. Here, we report that pannexin1 channels (Panx1) can be synaptically activated under physiological recording conditions in rodent acute hippocampal slices. Specifically, NMDA receptor (NMDAR)-mediated responses at the mossy fiber to CA3 pyramidal cell synapse were followed by a slow postsynaptic inward current that could activate CA3 pyramidal cells but was absent in Panx1 knockout mice. Immunoelectron microscopy revealed that Panx1 was localized near the postsynaptic density. Further, Panx1-mediated currents were potentiated by metabotropic receptors and bidirectionally modulated by burst-timing-dependent plasticity of NMDAR-mediated transmission. Lastly, Panx1 channels were preferentially recruited when NMDAR activation enters a supralinear regime, resulting in temporally delayed burst-firing. Thus, Panx1 can contribute to synaptic amplification and broadening the temporal associativity window for co-activated pyramidal cells, thereby supporting the auto-associative functions of the CA3 region.

INTRODUCTION

Pannexins are ion channels thought to exist primarily as hemichannels that exhibit broad expression profiles throughout the mammalian peripheral and central nervous system.[1,2] These ion channels exhibit characteristically large ionic conductances[3] and participate in various signaling pathways and metabolic processes.[4–6] In this capacity, pannexin channels are more than passive conduits to the extracellular milieu and display complex activity-dependent mechanisms regulating channel gating, conductance, and downstream signaling.[7] Mounting evidence has implicated pannexin1 (Panx1) channels in various pathological conditions ranging from epilepsy and ischemia to inflammation and neurodegeneration,[5] suggesting that the dysregulation of the mechanisms governing pannexin proteins can have significant pathological consequences. Owing to the severity of deficiencies in Panx1 function, this class of channels could play important physiological roles that have yet to be identified.

Within the brain, Panx1 channels are robustly expressed in the hippocampus, where they co-localize with PSD-95 in the CA1 region,[8] suggesting a potential physiological function at the synapse. Remarkably, Panx1 knockout animals exhibit significant learning impairments.[9–11] Panx1 antagonists and transgenic mice deficient for Panx1 can alter classical forms of plasticity at Schaeffer-collateral to CA1 pyramidal cell synapses (Sch-CA1).[9,12] Despite this evidence that Panx1 plays a role in hippocampal memory function, our mechanistic understanding of the physiological processes supported by Panx1 remains obscure. To evoke Panx1-mediated activity, most previous studies employed activation paradigms that are more closely related to pathological conditions,[13] and it has been difficult to directly evoke this activity under physiological conditions. In addition, prior work on Panx1 in the hippocampus has primarily focused on the CA1 region, whereas other subfields have been largely unexplored despite considerable expression levels in these regions.[14]

Here, we present evidence of synaptically driven Panx1 currents in cornu ammonis subfield 3 (CA3) pyramidal cells recorded in rat and mouse acute hippocampal slices. We found that NMDAR-mediated transmission drives Panx1 activity, most prominently at mossy fiber to CA3 pyramidal cell synapses (MF-CA3), which also depends on intracellular calcium. Activation of Panx1 generated large amplitude currents in the voltage-clamp recording configuration or burst-firing in current-clamp mode following the peak of the NMDAR-mediated response. Repetitive MF stimulation leading to the supralinear activation of NMDARs promoted the activation of Panx1, driving temporally delayed burst-firing output. Moreover, metabotropic receptors regulated Panx1 activity, and induction of burst timing-dependent NMDAR plasticity

[1]Department of Neurosurgery, Department of Neurology, Department of Biomedical Sciences, Center for Neural Science and Medicine, Cedars-Sinai Medical Center, Los Angeles, CA, USA
[2]Dominick P. Purpura Department of Neuroscience, Department of Psychiatry and Behavioral Sciences. Albert Einstein College of Medicine, Bronx, NY, USA
[3]Howard Hughes Medical Institute, Janelia Research Campus, Ashburn, VA, USA
[4]These authors contributed equally
[5]Lead contact
*Correspondence: pablo.castillo@einsteinmed.edu (P.E.C.), david.hunt@cshs.org (D.L.H.)
https://doi.org/10.1016/j.isci.2024.109681

resulted in concomitant modulation of Panx1 currents. Together, our results implicate neuromodulation and NMDAR plasticity at the MF-CA3 synapse as potent regulators of synaptically driven Panx1 activity. Thus, Panx1 can conditionally contribute to synaptic amplification by broadening the temporal associativity window for coactivated pyramidal cells, thereby supporting the auto-associative function of CA3 influencing hippocampal memory and "detonator" features of MF-CA3 synapses potentially contributing to network synchronization and epilepsy.

RESULTS

N-methyl-D-aspartate receptor secondary current activation in hippocampal CA3 pyramidal neurons

The present study was motivated by the unexpected observation while recording MF-CA3 NMDAR-mediated excitatory postsynaptic currents (NMDAR-EPSCs) in acute hippocampal slices (see STAR Methods for the recording conditions) whereby increasing the recording temperature from 25 ± 1°C to a more physiological 35 ± 1°C, NMDAR-EPSCs were often followed by a slow (off-peak) secondary current which we refer to as NMDAR-I_{2nd} (Figure 1A). No secondary current was observed at 25°C. NMDAR-I_{2nd} was only revealed at physiological temperature (35°C) in conjunction with NMDARs (Figures S1A and S1B), strongly suggesting that temperature plays a permissive role in the activation of the channel mediating this current. At 25°C, the MF-CA3 NMDAR-EPSC current-voltage relationship displayed the typical negative slope conductance from −70 to −40 mV. In contrast, a robust NMDAR-I_{2nd} (off-peak) became apparent when the recording temperature was set to 35°C at both positive and negative holding potentials (Figure 1B). NMDAR-I_{2nd} had a similar current-voltage relationship as the NMDAR-EPSC, except that it was larger, suggesting a large-conductance, non-selective cationic channel linked to the activation of NMDARs. NMDAR-I_{2nd} was stable throughout a 15-min recording period (Figure S1C). At the end of this recording period, bath application of the NMDAR competitive antagonist d-APV (25 μM) that competes with glutamate at the NMDAR ligand binding site or the irreversible open-channel blocker MK-801 (50 μM) abolished both NMDAR-EPSCs and NMDAR-I_{2nd} probability (Figure S1D), confirming that NMDAR-I_{2nd} is linked to NMDAR ionotropic activity. We also quantified the probability of observing NMDAR-I_{2nd} in each recording, which we found to be correlated with the amplitude of the synaptically evoked NMDAR-mediated EPSC (Figure 1C), further substantiating the notion that NMDAR activity triggers this secondary current activation.

To determine the functional significance of NMDAR-I_{2nd} on the output of CA3 pyramidal neurons, we performed whole-cell recordings in the current-clamp configuration. We used physiologically relevant bursts of presynaptic activity[15–20] by stimulating MFs with five pulses ranging in frequency from 2 to 100 Hz and measured the corresponding NMDAR-mediated EPSP amplitude and burst-firing probabilities for each frequency increment. NMDAR-mediated EPSPs increased supralinearly when normalized to the peak of the response after the fifth pulse of stimulation at 2 Hz for each cell (Figure 1D). Likewise, the probability of evoking a burst-firing response was greatest when NMDARs were maximally activated at 100 Hz. Conversely, delivering the same frequency ramp of stimulation while recording the kainate receptor (KAR)-mediated component of MF-CA3 synaptic transmission[21] (Figure 1E) exhibited a linear increase in EPSP amplitude (Figure 1F), suggesting that the supralinearity of NMDAR-EPSPs is unlikely to be due to a supralinear property of presynaptic release probability. Additionally, KAR-EPSPs of comparable level of depolarization to NMDAR-EPSPs only elicited single action potentials (Figure 1G) with equivalent stimulation conditions as when recording NMDAR-EPSPs, and all the KAR-EPSP-driven action potentials were short latency relative to the final pulse of synaptic stimulation. In contrast, spiking output mediated by NMDAR-EPSPs could be short latency, yet bursting preferentially occurred with a temporal delay that matched the time course of NMDAR-I_{2nd} (Figure 1H). In all, these results reflect the depolarization-dependent magnesium unblock of NMDARs that occurs predominantly at higher stimulation frequencies and leads to a higher probability of recruiting NMDAR-I_{2nd}, resulting in burst-firing output.

Pharmacological interrogation of N-methyl-D-aspartate receptor-I_{2nd} at mossy fiber to CA3 neuron synapses

An NMDAR-triggered secondary current was previously described in CA1 pyramidal neurons, where a transient exposure to exogenously applied NMDA activated an inward cationic current, a.k.a. NMDA post-exposure current.[22] This current was positively regulated by intracellular calcium and abolished in the absence of extracellular calcium, suggesting that NMDAR-mediated calcium influx is a key component of secondary current initiation. To determine the role of calcium for NMDAR-I_{2nd} initiation in CA3 pyramidal neurons, we first loaded these cells with the fast calcium chelator BAPTA (10 mM). This manipulation abolished NMDAR-I_{2nd} probability, leaving NMDAR-mediated EPSCs unaffected (Figure 2Ai). However, when cells were loaded with the calcium chelator EGTA (10 mM), which has slower binding kinetics than BAPTA, NMDAR-I_{2nd} was still present although slightly attenuated (Figure 2Aii), suggesting that "tight-coupling"[23] is necessary between the NMDAR and the channel mediating NMDAR-I_{2nd}. Consistent with this notion, we found that NMDAR-I_{2nd} was normally elicited but left NMDAR-EPSCs unaffected after depleting intracellular calcium stores by pre-incubating (30 min) and subsequently perfusing the reversible SERCA cyclopiazonic acid[24] (CPA) in the bath throughout the course of the experiment (Figure 2Aiii). Similar results were obtained using the non-reversible SERCA inhibitor thapsigargin (Figure S2). Together, these results indicate that calcium influx through the NMDAR is the primary contributor to the initiation of NMDAR-I_{2nd} in response to MF synaptic activation.

Given the current-voltage relationship and large amplitude exhibited by NMDAR-I_{2nd}, a charge carrier with large single-channel conductance, such as the gap junction family of channels,[25] emerged as a parsimonious candidate mediating this conductance. A recent study established a link between NMDAR-I_{2nd} and aberrant bursting in the CA1 region of the hippocampus.[13] While the activation paradigm employed in this study more closely emulates epileptiform activity instead of physiological activity patterns, the authors identified Panx1 as the channel contributing to this aberrant bursting activity. We therefore sought to test the hypothesis that Panx1 mediates NMDAR-I_{2nd} at MF synapses. To this end, we took a pharmacological approach. We first utilized the broad-spectrum gap junction blocker mefloquine (50 μM) yet observed no change in the occurrence of NMDAR-I_{2nd} and NMDAR-EPSCs (Figure 2Bi). We next turned to a structurally dissimilar

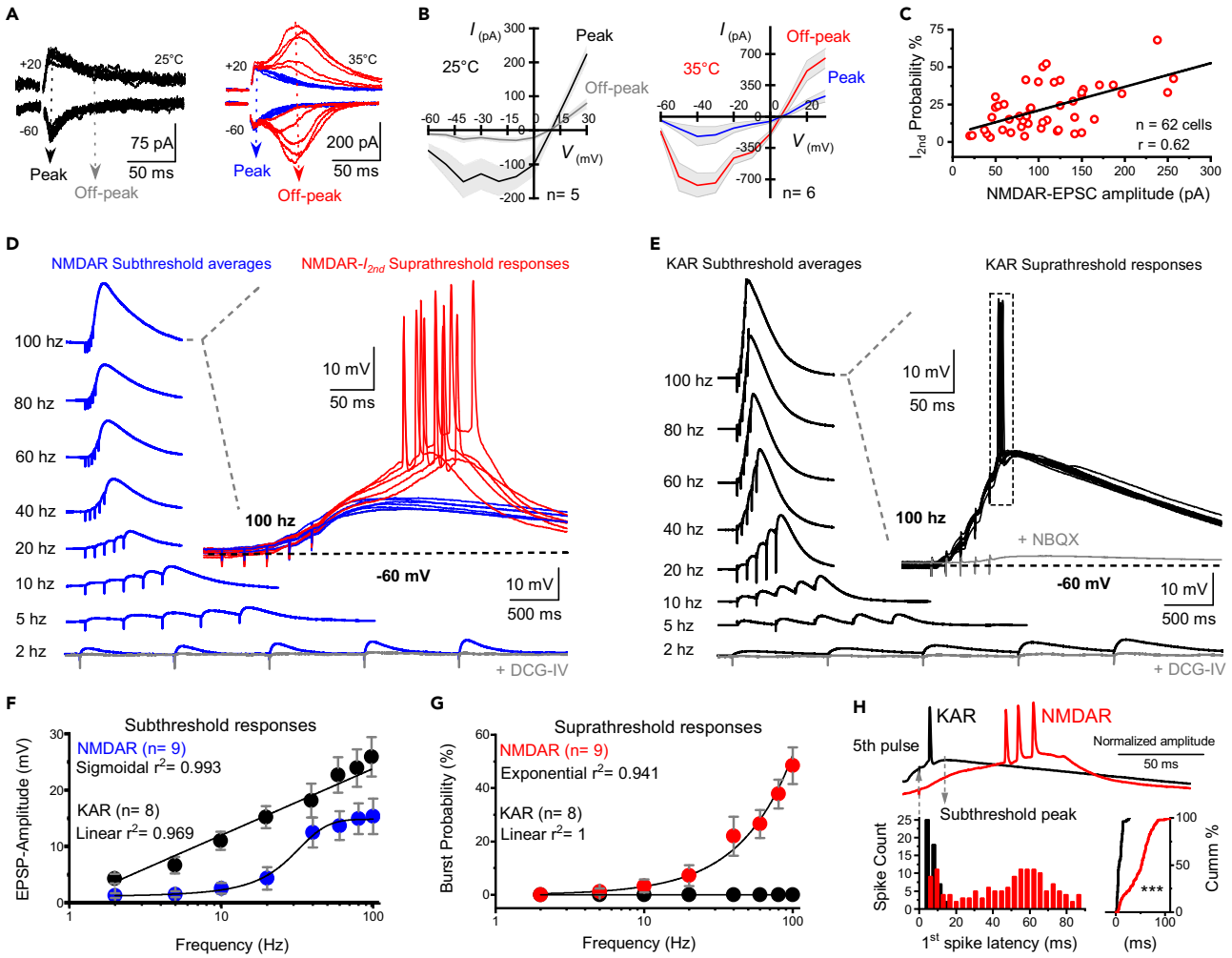

Figure 1. NMDAR secondary currents (NMDAR-I_{2nd}) at physiological temperature drove burst-firing output

(A) Representative traces at positive and negative holding potentials (black) from whole-cell recordings at 25°C and 35°C. No secondary currents were observed while monitoring NMDAR-mediated transmission at 25°C, but large amplitude delayed onset (off-peak) currents (red) were observed at 35°C.

(B) Current-voltage relationship for recordings at 25°C (n = 5 cells) where off-peak amplitude reflects the decay of NMDAR-mediated responses, and at 35°C (n = 6 cells) demonstrating large amplitude off-peak currents. Note the different Y axis range.

(C) A positive correlation was observed between the magnitude of the NMDAR-EPSC and the probability of NMDAR-I_{2nd} occurrence.

(D) Trace averages for a representative cell in which a 5-pulse burst of MF stimulation was delivered at the indicated frequencies, illustrating the subthreshold NMDAR-mediated EPSPs. Trace overlay of consecutive sweeps for 100 Hz stimulation highlighting the occurrence of suprathreshold bursting events (red, inset) intermittently observed with subthreshold NMDAR-EPSPs (blue, inset).

(E) Trace averages for a representative cell in which a 5-pulse burst of MF stimulation was delivered at the indicated frequencies, illustrating the subthreshold KAR-mediated EPSPs. Only short-latency individual spikes were observed (inset). We added 1μM DCG-IV, a group II mGluR agonist that attenuates mossy fiber transmission, at the end of the 2Hz train in each experiment to ensure responses were mediated by mossy fiber synapses (F) Summary data for subthreshold responses where the supralinearity of the NMDAR-EPSP (blue line, SEM gray, n = 9 cells) is shown relative to linearity KAR-mediated responses (n = 8 cells).

(G) Summary of suprathreshold responses illustrating the exponential increase in burst firing probability when NMDARs are in a supralinear regime.

(H) Summary of spike timing of NMDAR and KAR-mediated responses. NMDAR-mediated responses had both short-latency single spikes as well as delayed onset bursting (red), whereas KAR-mediated responses were associated with only short latency single spikes (black). (***p = 1.79 e−59). Student's paired-sample t-test was used to determine the significance between two groups. Data are presented as mean ± standard error of the mean (SEM).

compound, carbenoxolone, which can have functionally similar antagonistic effects on gap junction proteins.[26] Bath application of 30 μM carbenoxolone effectively abolished NMDAR-I_{2nd} (Figure 2Bii). Considering that a variety of factors can contribute to the pharmacological differences and specificity of canonical connexin and pannexin antagonists such as mefloquine and carbenoxolone, including isomeric structure and enantiomeric purity, these results indicate that pannexins rather than connexin channels were the more likely candidates mediating NMDAR-I_{2nd}, owing to the selective sensitivity to carbenoxolone over mefloquine.[27] Consistent with this hypothesis, we found that the specific

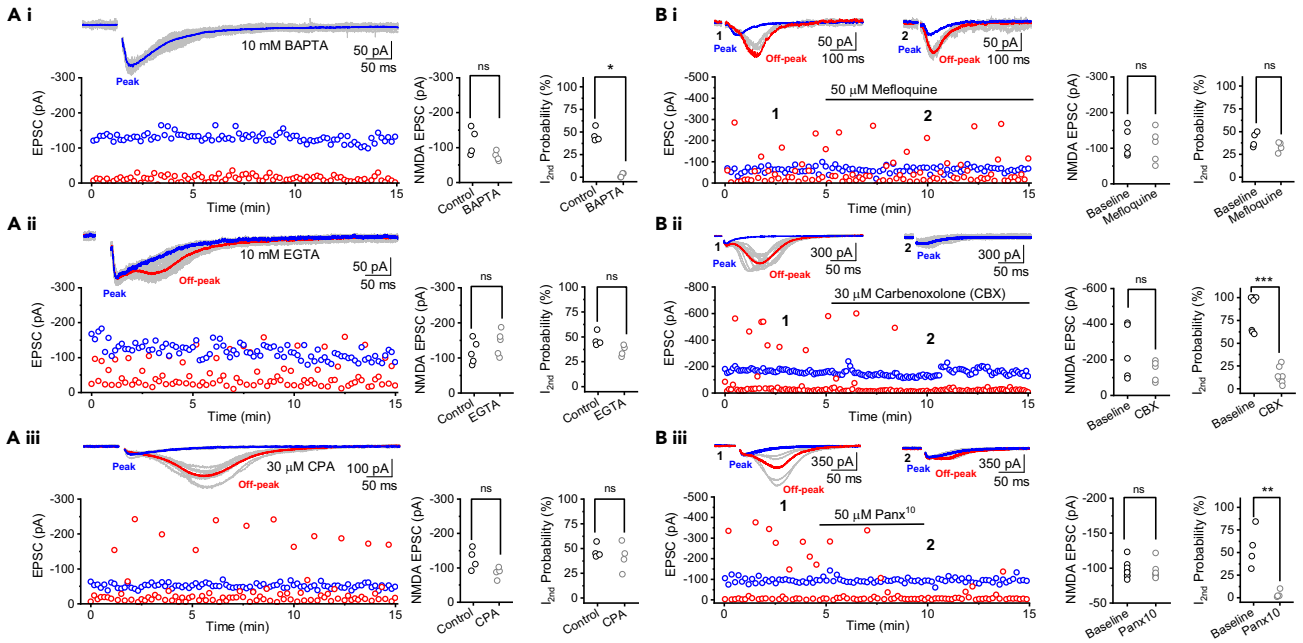

Figure 2. Calcium dependence and pharmacological interrogation identified Panx1 channels as mediating NMDAR-I_{2nd}

(Ai) Representative experiment showing that NMDAR-I_{2nd} was abolished when cells were intracellularly loaded with the fast calcium chelating agent BAPTA (10 mM). Individual trace overlay (gray) and average (blue) are shown above. No difference in NMDAR-EPSC was observed between control and in the presence of BAPTA (n = 4 cells, p = 0.11) while, NMDAR-I_{2nd} probability was abolished by BAPTA (n = 4 cells, *p = 0.02). (Aii) Representative experiment where cells were loaded intracellularly with EGTA (10 mM). No difference in NMDAR-EPSC (n = 5 cells, p = 0.30) and in NMDAR-I_{2nd} probability (n = 4 cells, p = 0.23) were detected between control and EGTA indicating that NMDAR-I_{2nd} was unaffected. (Aiii) Pre-incubation and continuous perfusion of slices with cyclopiazonic acid (CPA 30 μM) to deplete intracellular calcium stores did not impact NMDAR-I_{2nd}. Both NMDAR-EPSC (n = 4 cells, p = 0.26) and NMDAR-I_{2nd} probability (n = 4 cells, p = 0.77) were not affected by CPA, indicating that calcium from internal stores is not necessary to observe NMDAR-I_{2nd}.

(Bi) Representative experiment where the gap junction blocker Mefloquine (50 μM) was bath applied. No change in the probability of occurrence (n = 4 cells, p = 0.09) or amplitude of NMDAR-I_{2nd} (n = 5 cells, p = 0.56) was observed. Individual traces (gray) and averages for NMDAR-mediated responses (blue) and NMDAR-I_{2nd} (red) during baseline (1) and in the presence of Mefloquine (2) are shown above. (Bii) Representative experiment illustrating block of NMDAR-I_{2nd} by Carbenoxolone application (30 μM), while NMDAR-EPSCs were unaffected. As in (Bi), representative traces from the time points indicated (1, 2) are shown above. No change in NMDAR-EPSCs was observed (n = 5 cells, p = 0.22), but NMDAR-I_{2nd} probability was significantly reduced in the presence of Carbenoxolone (n = 7 cells, ***p = 4.9e-5). (Biii) Representative single experiment demonstrating that NMDAR-I_{2nd} can be blocked by the Panx1 inhibitory peptide (10Panx; 50 μM). As in (Bi) traces are shown above. No change in NMDAR-EPSC (n = 8 cells, p = 0.23) was observed, but the peptide significantly reduced NMDAR-I_{2nd} probability (n = 4 cells, **p = 0.01). All experiments were performed at 35°C. Student's paired-sample t-test was used to determine the significance between two groups. ns, no significant statistical difference.

Panx1 blocking peptide 10panx[13] robustly attenuated NMDAR-I_{2nd} but not NMDAR-EPSCs (Figure 2Biii). More extensive information regarding the properties of the drugs used in this study can be found in Table S1. Together, our results indicate that NMDAR activation at the MF-CA3 synapse triggers a calcium-dependent Panx1-mediated secondary conductance.

Anatomical localization of pannexin1 and synapse specificity of N-methyl-D-aspartate receptor-I_{2nd}

To provide anatomical evidence for the functional data suggesting that NMDARs activate Panx1 at MF-CA3 synapses, we endeavored to localize Panx1 to *stratum lucidum* in the CA3 region using an antibody that selectively binds to dendritically localized Panx1 (Mo503).[14] Histological staining of P20 rat brain tissue showed Panx1 immunoreactivity throughout the hippocampus (Figure S3A). We next sought to determine if Panx1-mediated NMDAR-I_{2nd} in CA3 pyramidal neurons was specific to MF synapses or if it could be triggered by stimulating other inputs, given that we observed Panx1 immuno-staining in other strata. To address this question, the stimulation intensity was tuned to yield, on average, an NMDAR-EPSC of 150 pA at different locations along the somatodendritic axis of CA3 neurons. By stimulating associational/commissural (AC) inputs in the CA3 *stratum radiatum*, we could observe NMDAR-I_{2nd}, albeit at a lower probability of occurrence than at MF synapses. Stimulating AC inputs in CA3 *stratum oriens* (Figure S3B) or stimulating CA1 Schaeffer collateral inputs in *stratum radiatum* yielded little to no NMDAR-I_{2nd} relative to MF-CA3 synapses (not shown). These observations are consistent with a different distribution of Panx1 along the somatodendritic axis of CA3 pyramidal neurons, as evidenced by Panx1 immunofluorescence in different CA3 strata (Figure S3B).

To obtain more detailed anatomical evidence and visualize the ultrastructural spatial distribution of Panx1, we performed immunogold labeling of Panx1 with the Mo503 antibody and imaged its localization at thorny excrescences with electron microscopy (Figure 3A). We

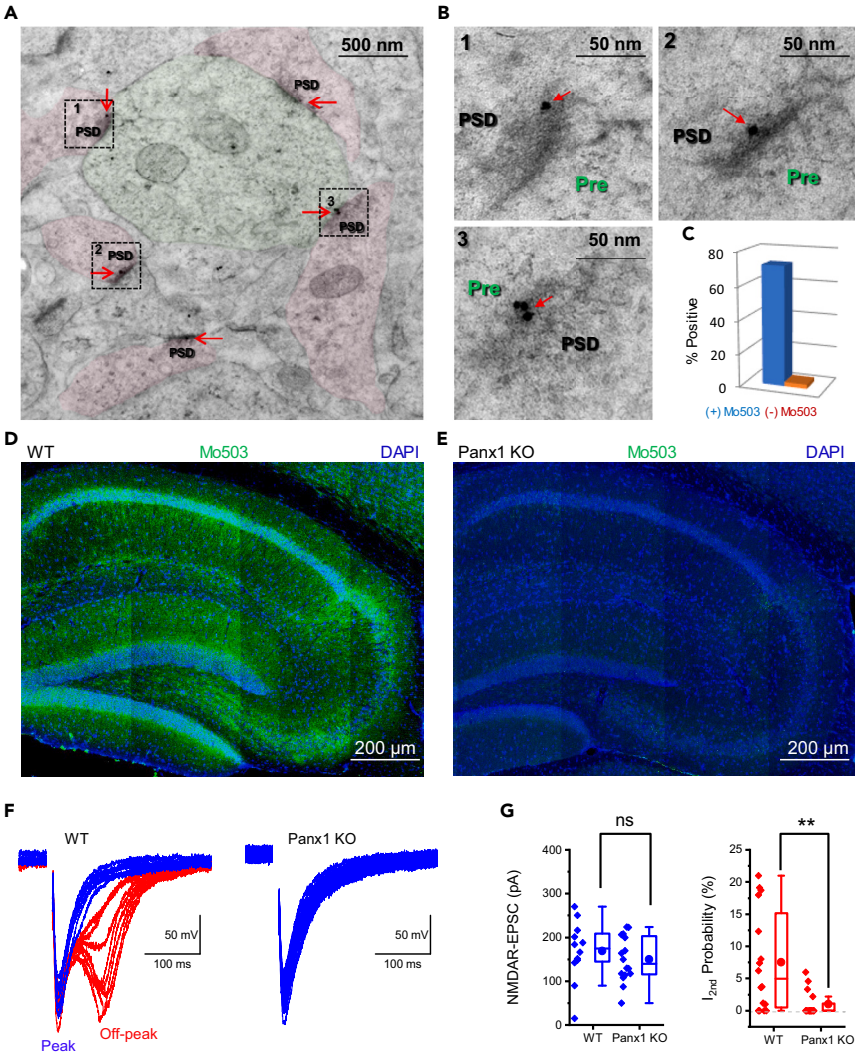

Figure 3. Postsynaptic localization of Panx1 and reduction of NMDAR-I_{2nd} in Panx1 knockout mice

(A) Immunoelectron microscopy of Panx1 at the thorny excrescences of pyramidal neurons in the CA3 region.The presynaptic MF bouton is highlighted in green and postsynaptic sites are outlined in pink. Red arrows point to gold puncta. Note single and double gold labeling proximal to PSD zones (scale bar: 500 nm).

(B) Enlarged view of dashed boxed regions shown in (A) illustrating the postsynaptic localization of Panx1 to the postsynaptic density of the thorny excrescence in CA3 principal cells (scale bar: 50 nm).

(C) Quantification of Panx1 positive postsynaptic sites with Panx1 antibody Mo503 and without this primary antibody; (+) Mo503 and (–) Mo503, respectively. The percentage reflects 8 presynaptic terminals and 27 postsynaptic thorns evaluated.

(D) Confocal microscopy images where wildtype (WT) mouse hippocampus was stained with Mo503 and DAPI demonstrating the expression of Panx1 throughout the hippocampus (scale bar: 200 µm).

(E) Panx1 knockout (Panx1 KO) mouse hippocampus stained with M0503 antibody and DAPI showing that Panx1 expression was markedly reduced in the Panx1 knockout mouse (scale bar: 200 µm).

(F) Representative traces from Wildtype and Panx1 knockout mice where secondary currents were absent.

(G) The probability of observing secondary currents was reduced in Panx1 knockout mice relative to wildtype littermates. While there was no difference in NMDAR-EPSCs between wildtype and knockout mice (blue, n = 16 cells, p = 0.43), the probability of generating Panx1 secondary currents was significantly reduced in knockout animals (red, n = 16 cells, $^{**}p$ = 0.007). Student's paired-sample t-test was used to determine the significance between two groups, data are expressed as mean ± minimum and maximum values (F and G).

evaluated 10 presynaptic MF boutons containing a total of 38 postsynaptic densities. (PSDs) and found Panx1 gold puncta near or in the PSD of the thorny excrescence at a frequency of approximately 70% (Figures 3A–3C). Additionally, using a Panx1 knockout mouse line,[14] we found little to no Panx1 immunoreactivity compared to wildtype controls (Figures 3D and 3E), confirming the specificity of the Mo503 antibody. Moreover, the probability of occurrence of NMDAR-I_{2nd} was drastically reduced in Panx1 knockout animals relative to interleaved wildtype controls (Figures 3F and 3G). Collectively, these data strongly support the hypothesis that Panx1 mediates NMDAR-I_{2nd} at MF-CA3 synapses.

Regulation of pannexin1-mediated N-methyl-D-aspartate receptor-I_{2nd} by metabotropic signaling

Activation of the type 5 metabotropic glutamate receptor (mGluR5) causes ATP release in the CA3 area through Panx1 hemichannels.[28] We therefore examined whether the activation of these receptors could facilitate Panx1-mediated NMDAR-I_{2nd} currents. Bath application of the group I metabotropic receptor (mGluR1 and mGluR5) agonist 3,5-Dihydroxyphenylglycine (DHPG, 1 μM) significantly increased NMDAR-I_{2nd} probability (Figure S4A). This increase was blocked by adding a selective antagonist of mGluR5 (MPEP) (Figure S4B) or by intracellularly loading the G protein blocker GDPβs (n = 9 cells, p = 0.83; data not shown), indicating a requirement for G protein-mediated signaling for the metabotropic regulation of NMDAR-I_{2nd}. We also examined whether Panx1 currents could be modulated by other G protein-coupled receptors, which, such as mGluR5, signal via Gq proteins. To this end, we performed similar experiments where either Carbachol (0.4 μM), which has broad spectrum activity across muscarinic receptor subtypes, or Oxalate (3 nM), which has greater selectivity for M1 muscarinic receptors and mimics the action of the endogenous ligand, were added to the bath after acquiring a 10-min baseline. Both agonists also increased NMDAR-I_{2nd} probability (Figures S4C and S4D). Notably, none of these pharmacological manipulations significantly affected the magnitude of NMDAR-EPSCs. Taken together, these results indicate that at least two different Gq-coupled receptors can potentiate Panx1-mediated NMDAR-I_{2nd}, contributing to a potential synergism with NMDAR activation.[29]

Bidirectional modulation of N-methyl-D-aspartate receptor-I_{2nd} via burst-timing dependent N-methyl-D-aspartate receptor plasticity

The exponential increase in the probability of NMDAR-I_{2nd} during high-frequency repetitive MF stimulation (Figure 1G) strongly suggests that presynaptic bursting activity, as it occurs *in vivo*,[15–20] could play a crucial role in the endogenous activation of NMDAR-I_{2nd}. Given that the NMDAR component of synaptic transmission can be potentiated at MF-CA3 synapses,[30,31] we tested whether the potentiation of NMDAR-mediated transmission at the MF-CA3 synapse could affect the activation of Panx1-mediated currents using a paradigm meant to mimic pre- and postsynaptic place field activity *in vivo*.[20,32] To this end, after establishing a baseline of MF-CA3 synaptic NMDAR-mediated responses, a pairing protocol was delivered consisting of five presynaptic pulses (50 Hz) followed 10 ms later by three suprathreshold current injections (1–1.5 nA, 1 ms duration, 100 Hz), which was repeated 50 times at 5 Hz[33] (Figure 4A). As expected, following this paring protocol, the NMDAR-mediated component of synaptic transmission was potentiated (Figure 4B). Concomitant with this NMDAR-LTP was a potentiation of the amplitude and frequency of the NMDAR-evoked Panx1 component of the compound EPSC (Figure 4C). Conversely, when we reverse the stimulation order to the post-pre protocol (Figure 4D), we could induce the depression of both the NMDAR-mediated component of MF-CA3 transmission[33] and the secondary Panx1-mediated slow component (Figures 4E and 4F). These data indicate that the activity-dependent plasticity of NMDARs is a potent regulator of Panx1-mediated NMDAR-I_{2nd}.

DISCUSSION

This study provides evidence of a synaptically evoked Panx1-mediated conductance that requires NMDAR activation and a postsynaptic calcium rise at MF-CA3 synapses (NMDAR-I_{2nd}). We demonstrate that the supralinear activation of NMDARs promotes temporally delayed burst-firing output, consistent with the exponential increase in NMDAR-I_{2nd} recruitment. We characterize the conditions for NMDAR-I_{2nd} activation and report that NMDAR-I_{2nd} can be elicited during basal synaptic transmission, indicating that Panx1-mediated NMDAR-I_{2nd} may play a physiological role at MF synapses. Additionally, we identify mechanisms of NMDAR-I_{2nd} modulation by metabotropic receptors and a burst-timing-dependent plasticity paradigm.

One of the conditions for observing Panx1-mediated NMDAR-I_{2nd} *in vitro* is the requirement for recording at or close to physiological temperature, indicating that the biophysical properties of Panx1 hemichannels have evolved to operate at physiological temperature for vertebrates.[34] Most previous experiments performed at room temperature may have overlooked the entire repertoire of mechanisms regulating synaptic transmission. Our data indicate that a higher, more physiological temperature is permissive, allowing NMDAR-I_{2nd} to be initiated by NMDAR activation. Although the mechanism by which temperature facilitates NMDAR-I_{2nd} remains to be identified, it may involve several processes, including changes in intracellular calcium dynamics and thermodynamic alterations to the Panx1 channel properties related to gating and conductivity.[6] In addition to the temperature requirement, the probability of observing secondary currents correlated with the magnitude of NMDAR-mediated transmission. However, not all cells conformed to this trend, where a small proportion did not exhibit any secondary conductance. There may be several biological and experimental factors that influence this variability. For example, our immune-gold electron microscopy suggests that not all PSDs are associated with Panx1 channels and could partially account for the range of secondary current amplitudes and probabilities observed in our experiments. Additionally, given the sensitivity of secondary current activation to intracellular calcium, the relative degree of intracellular dialysis could significantly impact the ability to observe Panx1-mediated secondary currents.

Another critical factor required for secondary conductance activation is a rise in intracellular calcium (but see[35]). Our data suggest that the calcium source primarily responsible is the NMDAR itself. Although NMDARs under pathological conditions can activate Panx1 channels in a metabotropic manner,[36] the suppression of NMDAR-I_{2nd} by the open channel blocker MK-801 suggests an ionotropic action under more physiological conditions. KAR-EPSPs, whose depolarization is expected to activate voltage-gated calcium channels, did not elicit any secondary currents, indicating that these channels do not significantly contribute to the activation of Panx1. While calcium from internal stores may contribute to secondary current activation, it is not required since NMDAR-I_{2nd} remained intact after depleting calcium from internal stores. The fact that BAPTA was far more effective than EGTA at blocking NMDAR-I_{2nd} activation strongly suggests a need for "tight-coupling"

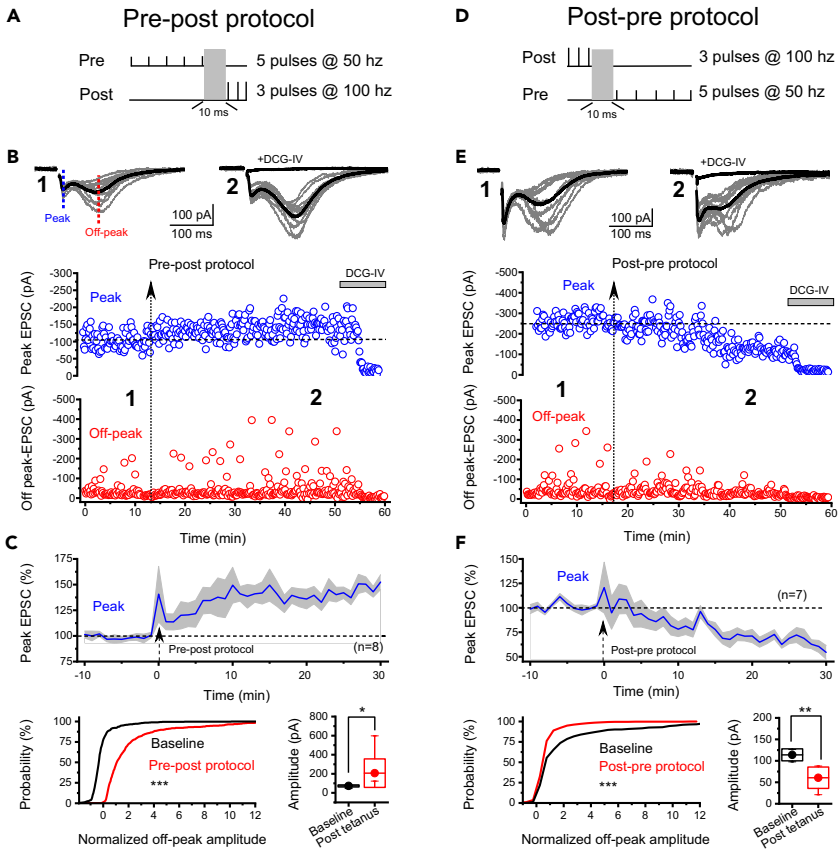

Figure 4. Bidirectional NMDAR plasticity modulated Panx1-mediated currents at MF-CA3 synapses

(A) Burst timing-dependent induction paradigm used to trigger the potentiation of NMDAR-mediated synaptic transmission (Pre-Post protocol), 5 presynaptic pulses (50 Hz) and 3 suprathreshold current injections (1–3 ms, 100 Hz) repeated 50 times at 5 Hz.

(B) Single experiment demonstrating the potentiation of NMDAR-mediated transmission (middle panel, blue) and a concomitant potentiation of Panx1 currents (Below, red) following the Pre-Post protocol (indicated by the vertical dashed arrow). Representative traces from the time points indicated (1, 2) are shown above.

(C) Summary data for 8 cells where the Pre-Post protocol was used to induce the potentiation of the NMDAR component (top panel, blue). Bottom, summary data indicating a significant increase in the probability (***p = 3.4e-25) and amplitude of Panx1 secondary currents (*p = 0.048) following the potentiation of NMDAR transmission.

(D) Burst timing-dependent induction paradigm used to trigger the depression of NMDAR-mediated transmission (Post-Pre protocol), 3 suprathreshold current injections (1 ms, 100 Hz) followed by 5 presynaptic pulses (50 Hz) repeated 50 times at 5 Hz.

(E) Single experiment where the depression of NMDAR-mediated transmission was induced by the Post-Pre protocol (middle panel, blue) and associated depression of Panx1 currents (Below, red) following the protocol. Representative traces from the time points indicated (1, 2) are shown above.

(F) Summary data for 7 cells where the Post-Pre protocol was used to induce the depression of the NMDAR component (top panel, blue). Bottom, summary data indicating a significant decrease in the probability (***p = 2.5e-5) and amplitude (**p = 0.006) following the depression of NMDAR transmission. All experiments were performed at 35°C. Student's paired-sample t test was used to determine significance between two groups. Data are presented as mean ± minimum and maximum values (C and F).

between NMDARs and Panx1 hemichannels where a micro- or nanodomain enables the activation of secondary currents. Consistent with this scenario, Panx1 was found in or near the postsynaptic density where NMDARs are also located (see also[8]). Because the open probability of pannexin channels can be directly modulated by calcium ion concentration,[37] gating of Panx1 hemichannels could be achieved by a direct interaction between free calcium ions and calcium-sensing domains on the channel itself. We cannot rule out that an intermediate calcium-binding protein or enzymatic modification[38] might drive the conformational changes needed for Panx1 channels to transition to the open state. The observed supralinearity of NMDAR activation and secondary current activation suggests that the cooperative binding of calcium ions to the channel could increase the open probability nonlinearly.

We have identified two Gq-coupled receptors that potentiate Panx1-mediated NMDAR-I_{2nd} activation. Specifically, we found that mGluR5 and M1 muscarinic acetylcholine receptor activation increased the amplitude and probability of occurrence of secondary currents. These findings align with previous studies indicating that the pharmacological activation of group-I metabotropic glutamate receptors (mGluRs) can activate an inward depolarizing current (I_{mGluR}).[39,40] Also, the pharmacological activation of mAChR has been shown to initiate depolarization events in acute slices resembling NMDAR-I_{2nd}.[41–43] Although the charge carrier mediating these currents remains unidentified, one possibility

would be transient receptor potential (TRP) channels, as mGluRs and mAChRs can activate these channels.[43] However, this possibility is unlikely given that NMDAR antagonism abolished both the NMDAR-mediated EPSC and NMDAR-I_{2nd}. Notably, a functional consequence of the metabotropic regulation of Panx1-mediated NMDAR-I_{2nd} is the ability to shift between single-spike and burst-firing output modes.[44]

The MF-CA3 synapse has long been hypothesized to play a "teaching" role in CA3 function.[45,46] The ability of a single synapse to discharge its postsynaptic pyramidal target[20] has earned this synapse the apt moniker of detonator. While several morphological and physiological attributes contribute to this functional property,[47] a complete understanding of the mechanisms endowing this unique ability has yet to be elucidated. Beyond the modulation by metabotropic receptors, we demonstrate that the activity-dependent plasticity of the NMDARs can potently and bidirectionally regulate Panx1-mediated NMDAR-I_{2nd}. Remarkably, there appeared to be a supralinear relationship between the degree of NMDAR-LTP and Panx1 potentiation, suggesting that relatively small changes in NMDAR-mediated Ca^{2+} influx could yield significant changes in the subsequent Panx1-mediated NMDAR-I_{2nd} activity. These findings indicate that one of the physiological roles of NMDAR plasticity at the MF synapse is to regulate the propensity for secondary current activation, thereby "tuning" the detonator properties. The observation described here that Panx1-mediated NMDAR-I_{2nd} can act as a potent mechanism of synaptic amplification based on NMDAR-mediated calcium influx directly contributes to the MF-CA3 synapse in its functional role of "detonator" of CA3 pyramids. The temporal delay in the activation of Panx1-mediated NMDAR-I_{2nd} increases the time over which active CA3 pyramids can strengthen recurrent synaptic connections, an essential component of the auto-associative function of the network. Indeed, recent work has shown that prolonged synaptic eligibility traces can enable plastic changes at more behaviorally relevant timescales[48] binding coactivated cells into an engram.

Although Panx1 can play a physiological role at the MF-CA3 synapse, it is important to highlight the consequences of Panx1 activity in the context of neuropathology.[2,49,50] Specifically, Panx1 has been implicated in epileptic activity and aberrant bursting in the hippocampus.[13,51] Temporal lobe structures, including the hippocampus, are often the site of origin for seizures. It follows that the upregulation of Panx1, by promoting the detonation of the CA3 area, can increase the excitability of a brain region involved in generating hypersynchronous activity patterns[52] and sharp-wave ripples.[53] Previous studies have shown that mitigating the functions of Panx1 can alleviate aberrant bursting and seizure activity.[13,51] Blockers of Panx1, such as probenecid, an FDA-approved drug for treating gout, could be repurposed as an anti-epileptic drug.

Limitations of the study

Here, we present data from slice physiology experiments in which we demonstrate the conditions and mechanisms for activating and regulating Panx1 channels, providing new insight into the role of Panx1 in synaptic physiology. As with any study conducted in acute brain slices, there remains a possibility that certain diffusible factors that are normally present in the extracellular milieu but are absent *in vitro* may contribute to the operation and regulation of Panx1 channels *in vivo*. In addition, our study utilizes specific strains of animals, and it remains to be determined whether the mechanisms we report here translate to other animal strains or higher mammals in which different channel subunit constituents could lead to additional mechanisms of the regulation of Panx1 channels. Moreover, the expression and precise subcellular localization of Panx1 channels may vary across species. Finally, while the pharmacological drugs and antibodies we utilized in our experiments exhibit specificity for Panx1, we cannot rule out the possibility that off-target effects may have impacted our results.

STAR★METHODS

Detailed methods are provided in the online version of this paper and include the following:

- KEY RESOURCES TABLE
- RESOURCE AVAILABILITY
  - Lead contact
  - Materials availability
  - Data and code availability
- EXPERIMENTAL MODEL AND STUDY PARTICIPANT DETAILS
  - Animals
- METHOD DETAILS
  - Brain slice preparation
  - Electrophysiology in brain slices
  - Immuno-gold electron microscopy
- QUANTIFICATION AND STATISTICAL ANALYSIS

SUPPLEMENTAL INFORMATION

Supplemental information can be found online at https://doi.org/10.1016/j.isci.2024.109681.

ACKNOWLEDGMENTS

We want to thank the Hunt and Castillo lab members for their constructive discussions on the data and helpful comments on the article. We also thank Eliana Scemes for the Mo503 antibody generated by Gina Sosinsky and the Panx1 KO mouse. This work was partially supported by

the National Institutes of Health (NIH, United States) grants R01 MH081935, R01 NS113600, and R01 MH1166673 to P.E.C. D.L.H was partially supported with a Grass Fellowship from the Grass Foundation. M.S. was supported by NIH R25 GM104547.

AUTHOR CONTRIBUTIONS

D.L.H and P.E.C, conceived the experimental design of the study. D.L.H, M.S, and C.R.S performed and analyzed electrophysiological experiments. W.L performed immune-gold electron microscopy experiments. D.L.H and P.E.C interpreted the results and wrote the article. All authors commented on the final version of the article.

DECLARATION OF INTERESTS

The authors declare no competing financial interests.

Received: September 28, 2023
Revised: February 23, 2024
Accepted: April 3, 2024
Published: April 6, 2024

REFERENCES

1. MacVicar, B.A., and Thompson, R.J. (2010). Non-junction functions of pannexin-1 channels. Trends Neurosci. *33*, 93–102. https://doi.org/10.1016/j.tins.2009.11.007.
2. Yeung, A.K., Patil, C.S., and Jackson, M.F. (2020). Pannexin-1 in the CNS: Emerging concepts in health and disease. J. Neurochem. *154*, 468–485. https://doi.org/10.1111/jnc.15004.
3. Sáez, J.C., Cisterna, B.A., Vargas, A., and Cardozo, C.P. (2015). Regulation of pannexin and connexin channels and their functional role in skeletal muscles. Cell. Mol. Life Sci. *72*, 2929–2935. https://doi.org/10.1007/s00018-015-1968-1.
4. Sandilos, J.K., and Bayliss, D.A. (2012). Physiological mechanisms for the modulation of pannexin 1 channel activity. J. Physiol. *590*, 6257–6266. https://doi.org/10.1113/jphysiol.2012.240911.
5. Madry, C., Haglerød, C., and Attwell, D. (2010). The role of pannexin hemichannels in the anoxic depolarization of hippocampal pyramidal cells. Brain *133*, 3755–3763. https://doi.org/10.1093/brain/awq284.
6. Chiu, Y.-H., Schappe, M.S., Desai, B.N., and Bayliss, D.A. (2018). Revisiting multimodal activation and channel properties of Pannexin 1. J. Gen. Physiol. *150*, 19–39. https://doi.org/10.1085/jgp.201711888.
7. Sandilos, J.K., Chiu, Y.-H., Chekeni, F.B., Armstrong, A.J., Walk, S.F., Ravichandran, K.S., and Bayliss, D.A. (2012). Pannexin 1, an ATP Release Channel, Is Activated by Caspase Cleavage of Its Pore-associated C-terminal Autoinhibitory Region. J. Biol. Chem. *287*, 11303–11311. https://doi.org/10.1074/jbc.M111.323378.
8. Zoidl, G., Petrasch-Parwez, E., Ray, A., Meier, C., Bunse, S., Habbes, H.-W., Dahl, G., and Dermietzel, R. (2007). Localization of the pannexin1 protein at postsynaptic sites in the cerebral cortex and hippocampus. Neuroscience *146*, 9–16. https://doi.org/10.1016/j.neuroscience.2007.01.061.
9. Prochnow, N., Abdulazim, A., Kurtenbach, S., Wildförster, V., Dvoriantchikova, G., Hanske, J., Petrasch-Parwez, E., Shestopalov, V.I., Dermietzel, R., Manahan-Vaughan, D., and Zoidl, G. (2012). Pannexin1 Stabilizes Synaptic Plasticity and Is Needed for Learning. PLoS One *7*, e51767. https://doi.org/10.1371/journal.pone.0051767.
10. Gajardo, I., Salazar, C.S., Lopez-Espíndola, D., Estay, C., Flores-Muñoz, C., Elgueta, C., Gonzalez-Jamett, A.M., Martínez, A.D., Muñoz, P., and Ardiles, Á.O. (2018). Lack of Pannexin 1 Alters Synaptic GluN2 Subunit Composition and Spatial Reversal Learning in Mice. Front. Mol. Neurosci. *11*, 114. https://doi.org/10.3389/fnmol.2018.00114.
11. Obot, P., Subah, G., Schonwald, A., Pan, J., Velíšek, L., Velíšková, J., Stanton, P.K., and Scemes, E. (2023). Astrocyte and neuronal Panx1 support long-term reference memory in mice. Preprint at BioRxiv. https://doi.org/10.1101/2023.01.16.524236.
12. Ardiles, A.O., Flores-MuÃ±oz, C., Toro-Ayala, G., CÃ¸rdenas, A.M., Palacios, A.G., MuÃ±oz, P., Fuenzalida, M., SÃ¸ez, J.C., and MartÃnez, A.D. (2014). Pannexin 1 regulates bidirectional hippocampal synaptic plasticity in adult mice. Front. Cell. Neurosci. *8*, 326. https://doi.org/10.3389/fncel.2014.00326.
13. Thompson, R.J., Jackson, M.F., Olah, M.E., Rungta, R.L., Hines, D.J., Beazely, M.A., MacDonald, J.F., and MacVicar, B.A. (2008). Activation of Pannexin-1 Hemichannels Augments Aberrant Bursting in the Hippocampus. Science *322*, 1555–1559. https://doi.org/10.1126/science.1165209.
14. Cone, A.C., Ambrosi, C., Scemes, E., Martone, M.E., and Sosinsky, G.E. (2013). A Comparative Antibody Analysis of Pannexin1 Expression in Four Rat Brain Regions Reveals Varying Subcellular Localizations. Front. Pharmacol. *4*, 6. https://doi.org/10.3389/fphar.2013.00006.
15. Danielson, N.B., Zaremba, J.D., Kaifosh, P., Bowler, J., Ladow, M., and Losonczy, A. (2016). Sublayer-Specific Coding Dynamics during Spatial Navigation and Learning in Hippocampal Area CA1. Neuron *91*, 652–665. https://doi.org/10.1016/j.neuron.2016.06.020.
16. GoodSmith, D., Chen, X., Wang, C., Kim, S.H., Song, H., Burgalossi, A., Christian, K.M., and Knierim, J.J. (2017). Spatial Representations of Granule Cells and Mossy Cells of the Dentate Gyrus. Neuron *93*, 677–690.e5. https://doi.org/10.1016/j.neuron.2016.12.026.
17. Senzai, Y., and Buzsáki, G. (2017). Physiological Properties and Behavioral Correlates of Hippocampal Granule Cells and Mossy Cells. Neuron *93*, 691–704.e5. https://doi.org/10.1016/j.neuron.2016.12.011.
18. Diamantaki, M., Frey, M., Berens, P., Preston-Ferrer, P., and Burgalossi, A. (2016). Sparse activity of identified dentate granule cells during spatial exploration. Elife *5*, e20252. https://doi.org/10.7554/eLife.20252.
19. Pernía-Andrade, A.J., and Jonas, P. (2014). Theta-Gamma-Modulated Synaptic Currents in Hippocampal Granule Cells In Vivo Define a Mechanism for Network Oscillations. Neuron *81*, 140–152. https://doi.org/10.1016/j.neuron.2013.09.046.
20. Henze, D.A., Wittner, L., and Buzsáki, G. (2002). Single granule cells reliably discharge targets in the hippocampal CA3 network *in vivo*. Nat. Neurosci. *5*, 790–795. https://doi.org/10.1038/nn887.
21. Castillo, P.E., Malenka, R.C., and Nicoll, R.A. (1997). Kainate receptors mediate a slow postsynaptic current in hippocampal CA3 neurons. Nature *388*, 182–186. https://doi.org/10.1038/40645.
22. Chen, Q.X., Perkins, K.L., Choi, D.W., and Wong, R.K. (1997). Secondary Activation of a Cation Conductance Is Responsible for NMDA Toxicity in Acutely Isolated Hippocampal Neurons. J. Neurosci. *17*, 4032–4036. https://doi.org/10.1523/JNEUROSCI.17-11-04032.1997.
23. Adler, E.M., Augustine, G.J., Duffy, S.N., and Charlton, M.P. (1991). Alien intracellular calcium chelators attenuate neurotransmitter release at the squid giant synapse. J. Neurosci. *11*, 1496–1507. https://doi.org/10.1523/JNEUROSCI.11-06-01496.1991.
24. Emptage, N.J., Reid, C.A., and Fine, A. (2001). Calcium Stores in Hippocampal Synaptic Boutons Mediate Short-Term Plasticity, Store-Operated Ca2+ Entry, and Spontaneous Transmitter Release. Neuron *29*, 197–208. https://doi.org/10.1016/S0896-6273(01)00190-8.
25. Barbe, M.T., Monyer, H., and Bruzzone, R. (2006). Cell-Cell Communication Beyond Connexins: The Pannexin Channels. Physiology *21*, 103–114. https://doi.org/10.1152/physiol.00048.2005.
26. Dahl, G., Qiu, F., and Wang, J. (2013). The bizarre pharmacology of the ATP release channel pannexin1. Neuropharmacology *75*, 583–593. https://doi.org/10.1016/j.neuropharm.2013.02.019.

27. Iglesias, R., Spray, D.C., and Scemes, E. (2009). Mefloquine Blockade of Pannexin1 Currents: Resolution of a Conflict. Cell Commun. Adhes. *16*, 131–137. https://doi.org/10.3109/15419061003642618.
28. Lopatář, J., Dale, N., and Frenguelli, B.G. (2015). Pannexin-1-mediated ATP release from area CA3 drives mGlu5-dependent neuronal oscillations. Neuropharmacology *93*, 219–228. https://doi.org/10.1016/j.neuropharm.2015.01.014.
29. Reiner, A., and Levitz, J. (2018). Glutamatergic Signaling in the Central Nervous System: Ionotropic and Metabotropic Receptors in Concert. Neuron *98*, 1080–1098. https://doi.org/10.1016/j.neuron.2018.05.018.
30. Kwon, H.-B., and Castillo, P.E. (2008). Long-term potentiation selectively expressed by NMDA receptors at hippocampal mossy fiber synapses. Neuron *57*, 108–120. https://doi.org/10.1016/j.neuron.2007.11.024.
31. Rebola, N., Lujan, R., Cunha, R.A., and Mulle, C. (2008). Adenosine A2A Receptors Are Essential for Long-Term Potentiation of NMDA-EPSCs at Hippocampal Mossy Fiber Synapses. Neuron *57*, 121–134. https://doi.org/10.1016/j.neuron.2007.11.023.
32. Jung, M.W., and McNaughton, B.L. (1993). Spatial selectivity of unit activity in the hippocampal granular layer. Hippocampus *3*, 165–182. https://doi.org/10.1002/hipo.450030209.
33. Hunt, D.L., Puente, N., Grandes, P., and Castillo, P.E. (2013). Bidirectional NMDA receptor plasticity controls CA3 output and heterosynaptic metaplasticity. Nat. Neurosci. *16*, 1049–1059. https://doi.org/10.1038/nn.3461.
34. Abascal, F., and Zardoya, R. (2013). Evolutionary analyses of gap junction protein families. Biochim. Biophys. Acta *1828*, 4–14. https://doi.org/10.1016/j.bbamem.2012.02.007.
35. Ma, W., Hui, H., Pelegrin, P., and Surprenant, A. (2009). Pharmacological Characterization of Pannexin-1 Currents Expressed in Mammalian Cells. J. Pharmacol. Exp. Ther. *328*, 409–418. https://doi.org/10.1124/jpet.108.146365.
36. Weilinger, N.L., Lohman, A.W., Rakai, B.D., Ma, E.M.M., Bialecki, J., Maslieieva, V., Rilea, T., Bandet, M.V., Ikuta, N.T., Scott, L., et al. (2016). Metabotropic NMDA receptor signaling couples Src family kinases to pannexin-1 during excitotoxicity. Nat. Neurosci. *19*, 432–442. https://doi.org/10.1038/nn.4236.
37. Locovei, S., Wang, J., and Dahl, G. (2006). Activation of pannexin 1 channels by ATP through P2Y receptors and by cytoplasmic calcium. FEBS Lett. *580*, 239–244. https://doi.org/10.1016/j.febslet.2005.12.004.
38. López, X., Palacios-Prado, N., Güiza, J., Escamilla, R., Fernández, P., Vega, J.L., Rojas, M., Marquez-Miranda, V., Chamorro, E., Cárdenas, A.M., et al. (2021). A physiologic rise in cytoplasmic calcium ion signal increases pannexin1 channel activity via a C-terminus phosphorylation by CaMKII. Proc. Natl. Acad. Sci. USA *118*, e2108967118. https://doi.org/10.1073/pnas.2108967118.
39. Chuang, S.-C., Bianchi, R., and Wong, R.K. (2000). Group I mGluR Activation Turns on a Voltage-Gated Inward Current in Hippocampal Pyramidal Cells. J. Neurophysiol. *83*, 2844–2853. https://doi.org/10.1152/jn.2000.83.5.2844.
40. Gee, C.E., Benquet, P., and Gerber, U. (2003). Group I metabotropic glutamate receptors activate a calcium-sensitive transient receptor potential-like conductance in rat hippocampus. J. Physiol. *546*, 655–664. https://doi.org/10.1113/jphysiol.2002.032961.
41. Bianchi, R., and Wong, R.K. (1994). Carbachol-induced synchronized rhythmic bursts in CA3 neurons of guinea pig hippocampus *in vitro*. J. Neurophysiol. *72*, 131–138. https://doi.org/10.1152/jn.1994.72.1.131.
42. Fujisawa, S., Matsuki, N., and Ikegaya, Y. (2006). Single Neurons Can Induce Phase Transitions of Cortical Recurrent Networks with Multiple Internal States. Cereb. Cortex *16*, 639–654. https://doi.org/10.1093/cercor/bhj010.
43. Guérineau, N.C., Bossu, J.L., Gähwiler, B.H., and Gerber, U. (1995). Activation of a nonselective cationic conductance by metabotropic glutamatergic and muscarinic agonists in CA3 pyramidal neurons of the rat hippocampus. J. Neurosci. *15*, 4395–4407. https://doi.org/10.1523/JNEUROSCI.15-06-04395.1995.
44. Durstewitz, D., and Seamans, J.K. (2006). Beyond bistability: Biophysics and temporal dynamics of working memory. Neuroscience *139*, 119–133. https://doi.org/10.1016/j.neuroscience.2005.06.094.
45. Marr, D. (1971). Simple memory: a theory for archicortex. Philos. Trans. R. Soc. Lond. B Biol. Sci. *262*, 23–81. https://doi.org/10.1098/rstb.1971.0078.
46. McNaughton, B.L., and Morris, R.G.M. (1987). Hippocampal synaptic enhancement and information storage within a distributed memory system. Trends Neurosci. *10*, 408–415. https://doi.org/10.1016/0166-2236(87)90011-7.
47. Nicoll, R.A., and Schmitz, D. (2005). Synaptic plasticity at hippocampal mossy fibre synapses. Nat. Rev. Neurosci. *6*, 863–876. https://doi.org/10.1038/nrn1786.
48. Bittner, K.C., Milstein, A.D., Grienberger, C., Romani, S., and Magee, J.C. (2017). Behavioral time scale synaptic plasticity underlies CA1 place fields. Science *357*, 1033–1036. https://doi.org/10.1126/science.aan3846.
49. Seo, J.H., Dalal, M.S., and Contreras, J.E. (2021). Pannexin-1 Channels as Mediators of Neuroinflammation. Int. J. Mol. Sci. *22*, 5189. https://doi.org/10.3390/ijms22105189.
50. Silverman, W.R., de Rivero Vaccari, J.P., Locovei, S., Qiu, F., Carlsson, S.K., Scemes, E., Keane, R.W., and Dahl, G. (2009). The Pannexin 1 Channel Activates the Inflammasome in Neurons and Astrocytes. J. Biol. Chem. *284*, 18143–18151. https://doi.org/10.1074/jbc.M109.004804.
51. Santiago, M.F., Veliskova, J., Patel, N.K., Lutz, S.E., Caille, D., Charollais, A., Meda, P., and Scemes, E. (2011). Targeting Pannexin1 Improves Seizure Outcome. PLoS One *6*, e25178. https://doi.org/10.1371/journal.pone.0025178.
52. Hendricks, W.D., Westbrook, G.L., and Schnell, E. (2019). Early detonation by sprouted mossy fibers enables aberrant dentate network activity. Proc. Natl. Acad. Sci. USA *116*, 10994–10999. https://doi.org/10.1073/pnas.1821227116.
53. Buzsáki, G. (2015). Hippocampal sharp wave-ripple: A cognitive biomarker for episodic memory and planning. Hippocampus *25*, 1073–1188. https://doi.org/10.1002/hipo.22488.
54. Kumar, A. (2011). Long-Term Potentiation at CA3–CA1 Hippocampal Synapses with Special Emphasis on Aging, Disease, and Stress. Front. Aging Neurosci. *3*, 7.

STAR★METHODS

KEY RESOURCES TABLE

REAGENT or RESOURCE	SOURCE	IDENTIFIER
Antibodies		
Mouse monoclonal antibody Mo503	G.E. Sosinsky, University of California at San Diego; California; USA	Cat# Mo503, RRID: AB_10013323
Goat anti-mouse IgG conjugated to 6-nm gold particles	Jackson ImmunoResearch	Cat# 115-195-146; RRID: AB_2338728
Non-immune mouse IgG	Jackson ImmunoResearch	Cat# 015-000-003; RRID: AB_2337188
Chemicals, peptides, and recombinant proteins		
DCG-IV	Tocris Bioscience	Cat# 0975
d-APV	Tocris Bioscience	Cat# A8054
NBQX	Tocris Bioscience	Cat# 0373
(+)-MK-801 maleate	Tocris Bioscience	Cat# 0924
Picrotoxin	Tocris Bioscience	Cat# 1128
CGP55845	Tocris Bioscience	Cat# 1248
GYKI53655 hydrochloride	Tocris Bioscience	Cat# 2555
(RS) -3,5-DHPG	Tocris Bioscience	Cat# 0342
2-Methyl-6-(phenylethynyl)pyridine hydrochloride (MPEP)	Tocris Bioscience	Cat# 1212
Guanosine 5′-[β-thio] diphosphate trilithium salt (GDPβs)	Sigma-Aldrich	Cat# G7637
Carbamoylcholine chloride (Carbachol)	Sigma-Aldrich	Cat# C4382
Xanomeline Oxalate	Sigma-Aldrich	Cat# 5058160001
CGS-21680 hydrochloride	Sigma-Aldrich	Cat# 119137
BAPTA	Tocris Bioscience	Cat# 2786
EGTA	Tocris Bioscience	Cat# 2807
Cyclopiazonic acid (CPA)	Tocris Bioscience	Cat# 1235
Mefloquine hydrochloride	Sigma-Aldrich	Cat# M2319
Carbenoxolone disodium salt	Sigma-Aldrich	Cat# C4790
Panx10	Tocris Bioscience	Cat# 3348
Thapsigargin	Tocris Bioscience	Cat# 1138
Critical commercial assays		
HQ silver kit	Nanoprobes	Cat# 2012-45ML
Experimental models: Organisms/strains		
Wistar rats	Charles River	Cat# 003
Pannexin1 knockout mice	MMRRC	Cat# 048960-UCD; RRID:MMRRC_048960-UCD
Software and algorithms		
pClamp 11.1	Molecular Devices	https://www.moleculardevices.com/
IgorPro	WaveMetrics	https://www.wavemetrics.com/
OriginPro 2021b	OriginLab	https://www.originlab.com/

RESOURCE AVAILABILITY

Lead contact

Further information and requests for resources and reagents should be directed to and will be fulfilled by the lead contact, David Hunt (david.hunt@cshs.org).

Materials availability

This study did not generate new unique reagents.

Data and code availability

- All data reported in this paper will be shared by the lead contact upon request.
- This paper does not report original code.
- Any additional information required to reanalyze the data reported in this paper is available from the lead contact upon request.

EXPERIMENTAL MODEL AND STUDY PARTICIPANT DETAILS

Animals

Animal handling and use followed a protocol approved by the Institutional Animal Care and Use Committee of Albert Einstein College of Medicine, Cedars-Sinai Medical Center, and Janelia Research Campus in accordance with the National Institutes of Health Guide for the Care and Use of Laboratory Animals. Hippocampal slices were prepared from both male and female Wistar rats (17-30 days old) and Panx1 knockout mice[51] (15-30 days old).

METHOD DETAILS

Brain slice preparation

Animals were deeply anesthetized with isoflurane and decapitated. The brain was rapidly removed into a chilled cutting solution consisting of (in mM): 215 sucrose, 2.5 KCl, 20 glucose, 26 $NaHCO_3$, 1.6 NaH_2PO_4, 1 $CaCl_2$, 4 $MgCl_2$, and 4 $MgSO_4$. Hippocampi were dissected out and cut into 400 μm thick transverse sections on a DTK-2000 vibrating microslicer (Dosaka EM Co., Ltd., Japan) or a VT1200s microslicer (Leica Microsystems Co., Ltd., Germany). The cutting solution was slowly exchanged with artificial cerebrospinal fluid (ACSF) containing (in mM): 124 NaCl, 2.5 KCl, 10 glucose, 26 $NaHCO_3$, 1.0 NaH_2PO_4, 2.5 $CaCl_2$, and 1.3 $MgCl_2$. Both cutting and ACSF solutions were saturated with 95% O_2 and 5% CO_2 (pH 7.4). The slices were incubated at room temperature for at least 1 hr before recording. The slices were then transferred as needed to a submersion-type recording chamber and were perfused with ACSF (2 ml/min).

Electrophysiology in brain slices

Whole-cell recordings of CA3 pyramidal cells were obtained using standard techniques. To maximize cell health and recording stability, cells deep below the surface of the slice were recorded "semi-blind". The recording pipette resistance ranged between 3 and 4 MΩ. Series resistance (8–15 MΩ) and input resistance were monitored throughout each voltage-clamp recording with 80 ms, -4 mV steps. Recordings with >10% change in series or input resistance were systematically excluded. The pipette solution for all recordings contained (in mM): 135 K-gluconate, 5 KCl, 0.4 $CaCl_2$, 0.1 EGTA, 10 HEPES, 10 glucose, 5 MgATP, and 0.4 Na_3GTP. In current clamp mode, this internal solution yielded a resting membrane potential that ranged from -69 to -58 mV, uncorrected for the liquid junction potential. The maximum recording time after dissection was 6 hr. The recording temperature was set to 35.0°C ± 0.1°C using a TC-344B dual-channel temperature controller (Warner Instruments, Inc, Hamden, CT, USA). Synaptic afferents were activated by monopolar stimulation delivered via a patch-type pipette broken to a tip diameter of ≈10 μm and filled with ACSF. This stimulating electrode was placed in the dentate gyrus cell body layer to activate MFs and in the CA3 *s. radiatum* (100-150 μm apical to *s. lucidum*) to activate AC fibers. AC fibers projecting to the basal dendrites of CA3 neurons were activated by placing the stimulation electrode in *s. oriens*. The baseline stimulation rate was 0.1 Hz for all experiments. To confirm that the activated afferents were not significantly contaminated by AC inputs, 1 μM DCG-IV, a group II mGluR agonist that blocks MF but not AC synaptic transmission, was applied at the end of every experiment (except where d-APV is added), and the data were accepted only if synaptic responses were reduced by more than 90%. The synaptic response remaining in DCG-IV was then subtracted from all previous responses before further analysis to isolate MF-specific synaptic activity. Unless otherwise noted, NMDAR-EPSCs were elicited by 2-3 pulse stimulation (5 ms or 40 ms inter-stimulus interval, ISI) in the presence of 10 μM NBQX, 100 μM picrotoxin, and 3 μM CGP55845, to block AMPA/KA, $GABA_A$ and $GABA_B$ receptors, respectively, while voltage-clamping to -50 mV. For KAR-EPSCs, the selective AMPAR antagonist GYKI53655 (30 μM) was used, and cells were voltage-clamped to -70 mV. The identity of KAR-EPSCs was confirmed by adding 10 μM NBQX at the end of each experiment. KAR-mediated MF-CA3 EPSCs were evoked by single stimulation or a 5-pulse train in the dentate gyrus. AMPAR-EPSCs were elicited using single-pulse stimulation, recorded in the absence of drugs in the bath while voltage clamping at -70 mV (i.e., at $GABA_AR$ reversal), and included in the analysis based on their characteristically fast kinetics (~1 ms rise time). A full description of the drugs used in this study can be found in Table S1. The LTP experiments were performed using a theta burst stimulation (TBS), which consisted of three trains delivered every 20 seconds, and every train was formed by ten stimulus epochs delivered at 5 Hz (200 ms), with each epoch consisting of four pulses at 100 Hz.[54] All experiments were executed with a MultiClamp 700B (Axon Instruments/Molecular Devices, Union City, CA, USA). Electrophysiological data were filtered (2.5 KHz) digitized (3–5 KHz) and analyzed using custom-made software for IgorPro (Wavemetrics Inc., Lake Oswego, OR, USA).

Immuno-gold electron microscopy

P17 Wistar rat brains were transcardially perfusion fixed in 4% paraformaldehyde and 0.2% glutaraldehyde in 0.1 M phosphate buffer (pH 7.4), followed by overnight immersion in the same fixative. The brains were cut into 120-μm-thick slices with a vibratome, and the CA3 area of the hippocampus was excised. The samples were subjected in 20% BSA and transferred to HPF Compact 01 high-pressure-freezing machine (M. Wohlwend GmbH) for cryo-immobilization. The samples were stored in liquid nitrogen, and freeze substituted in acetone containing 0.1% uranyl acetate plus 3% distilled water in a freeze substitution unit (Leica EM AFS2, Leica Microsystems) at −90°C for 72 hours. Afterward, the temperature was brought up slowly to −50°C; the brain samples were rinsed with pure acetone and infiltrated with 30%, 50%, and 70% Lowicryl HM20 resin in acetone for 1 hour each, followed by 100% HM20 resin overnight. Samples were embedded in Lowicryl HM20 and UV polymerized for 2 days at −50°C and 2 days at 20°C. Postembedding immunogold labeling was performed on ultrathin HM20 sections (65 nm) of the brains to detect Panx1 using mouse monoclonal antibody Mo503. The ultrathin sections were conditioned in the blocking buffer containing 1% bovine serum albumin (w/v, Sigma-Aldrich, St. Louis, MO) in PBS for 10 min at room temperature, and then incubated overnight at 4°C with Mo503 (diluted 1:10) in blocking buffer. After extensive rinsed in PBS, the sections were incubated for 1 h at 35°C with goat anti-mouse IgG conjugated to 6-nm gold particles (Jackson ImmunoResearch, West Grove, PA) diluted to 1:40 in block buffer. The samples were rinsed in PBS, fixed with 1% (v/v) glutaraldehyde in PBS for 10 min. Finally, the gold particles were amplified with silver enhancement (HQ silver kit from Nanoprobes, Yaphank, NY) for 4 min at room temperature and contrast stained with 3% UA and Sato's triple lead. Electron micrographs were taken with a FEI Tecnai 20 Twin electron microscope operating at 80 kV. Negative controls were performed with omitting or replacing the primary antibody with non-immune mouse IgG (Jackson ImmunoResearch, West Grove, PA). Micrographs from Panx1 labeling and two control groups were taken at the original magnification of x 115,000. The percentage of gold particle labeling synapses was estimated over the synapses of MF bouton (MFBs).

QUANTIFICATION AND STATISTICAL ANALYSIS

For experiments performed in rats, data was collected in blocked fashion according to pharmacological or electrical manipulation with interleaved controls and was not blinded. For experiments performed in Panx1 knockout mice data collection and analysis was performed blinded to genotype. Generally, no data were excluded in this study. However, recordings with greater than 20% change in input or series resistance were systematically excluded from analysis. All statistical analysis was performed using OriginPro 2021b (OriginLab Corp., Northampton, MA). Normality was determined by a Shapiro-Wilk test at a significance of 0.05 for parametric statistical comparisons. Non-parametric comparisons were performed by a Mann-Whitney U test or Wilcoxon Rank Sum test. The magnitude of plasticity was always assessed relative to interleaved controls and was quantified by averaging synaptic responses, for 10 min periods right before and 20-30 min after the induction protocol. The probability of observing secondary currents (NMDAR-I_{2nd} probability) was calculated by taking the distribution of off-peak measurements for a given time epoch (for example, the baseline period before drug application) and quantifying the mean and standard deviation of this distribution (see Figure S1E). We defined the threshold for a secondary current (see Figure S1F) to be one standard deviation above the mean of the distribution for a given time period. We then divided the number of secondary current occurrences by the total number of synaptic responses in the appropriate time epoch. The probability values were then compared between baseline or control and drug application experiments. NMDAR amplitude was obtained by calculating the mean of each representative time-course experiment. Statistical significance between means was calculated using Student's t-test. A paired t-test was used to compare baseline with responses post-induction, whereas an unpaired t-test was used to compare experimental manipulations with interleaved control experiments. In all figures, error bars indicate ± standard error of the mean (SEM), and averaged traces include 15–30 consecutive individual responses.